Journal of Structural Geology 31 (2009) 910–925

Contents lists available at ScienceDirect

Journal of Structural Geology

journal homepage: www.elsevier.com/locate/jsg

Origin of fault domains and fault-domain boundaries (transfer zones and accommodation zones) in extensional provinces: Result of random nucleation and self-organized fault growth

Roy W. Schlische*, Martha Oliver Withjack

Department of Earth & Planetary Sciences, Rutgers University, 610 Taylor Road, Piscataway, NJ 08854-8066, USA

ARTICLE INFO

Article history:
Received 2 May 2007
Received in revised form 15 May 2008
Accepted 16 September 2008
Available online 9 October 2008

Keywords:
Normal faults
Transfer zones/accommodation zones
Extension
Experimental modeling
Fault growth

ABSTRACT

In many extensional provinces, large normal faults dip in the same direction forming fault domains. Features variously named transfer faults, transfer zones, and accommodation zones (hereafter non-genetically referred to as fault-domain boundaries) separate adjacent fault domains. Experimental modeling of distributed extension provides insights on the origin, geometry, and evolution of these fault domains and fault-domain boundaries. In our scaled models, a homogeneous layer of wet clay or dry sand overlies a latex sheet that is stretched orthogonally or obliquely between two rigid sheets. Fault domains and fault-domain boundaries develop in all models in both map view and cross-section. The number, size, and arrangement of fault domains as well as the number and orientation of fault-domain boundaries are variable, even for models with identical boundary conditions. The fault-domain boundaries in our models differ profoundly from those in many published conceptual models of transfer/accommodation zones. In our models, fault-domain boundaries are broad zones of deformation (not discrete strike-slip or oblique-slip faults), their orientations are not systematically related to the extension direction, and they can form spontaneously without any prescribed pre-existing zones of weakness. We propose that fault domains develop because early-formed faults perturb the stress field, causing new nearby faults to dip in the same direction (self-organized growth). As extension continues, faults from adjacent fault domains propagate toward each another. Because opposite-dipping faults interfere with one another in the zone of overlap, the faults stop propagating. In this case, the geometry of the domain boundaries depends on the spatial arrangement of the earliest formed faults, a result of the random distribution of the largest flaws at which the faults nucleate.

1. Introduction

Fault domains, in which all or most normal faults dip in the same direction, are common in extensional provinces (e.g., Mandl, 1987; Morley et al., 1990; Carbotte and Macdonald, 1990; Faulds and Varga, 1998). This style of faulting is termed 'domino-style faulting' or 'bookshelf faulting' (e.g., Emmons and Garrey, 1910; Morton and Black, 1975; Proffett, 1977; Wernicke and Burchfiel, 1982), because the fault blocks between the normal faults are tilted in the opposite direction of the fault-dip direction. The tilted fault blocks have undergone a rotation with the blocks rotating to steeper dips and the faults rotating to gentler dips as strain increases. Fault domains develop at many scales ranging from centimeters to meters (e.g., Fig. 1 from the Danville rift basin, eastern North America), to kilometers (e.g., Fig. 2A from the Gulf of Thailand), to tens of kilometers (e.g., Fig. 2B from the Suez rift basin). *Fault-domain boundaries* are zones that separate fault domains from either unfaulted regions (Fig. 1B and C) or from adjacent fault domains (Fig. 2A and B). Fault-domain boundaries are variously referred to as transfer faults, transfer zones, and accommodation zones (e.g., Morley et al., 1990; Faulds and Varga, 1998; Peacock et al., 2000). Because the nomenclature is in a state of flux (cf. Faulds and Varga, 1998; Peacock et al., 2000), we prefer to give these features a descriptive, rather than a genetic, name.

Fault-domain boundaries are present in many extensional provinces. In the Gulf of Thailand (Fig. 2A), N-striking normal faults form domains of E- and W-dipping faults (Kornsawan and Morley, 2002). In map view, the fault-domain boundaries are both parallel and oblique to the strike of the normal faults. In cross-section (trending perpendicular to the strike of the normal faults), the fault-domain boundaries have either horst or graben geometries. The horst geometries are relatively simple, whereas the graben geometries are complex, consisting of numerous fault terminations

* Corresponding author.
E-mail addresses: schlisch@rci.rutgers.edu (R.W. Schlische), drmeow3@rci.rutgers.edu (M.O. Withjack).

0191-8141/$ – see front matter © 2008 Elsevier Ltd. All rights reserved.
doi:10.1016/j.jsg.2008.09.005

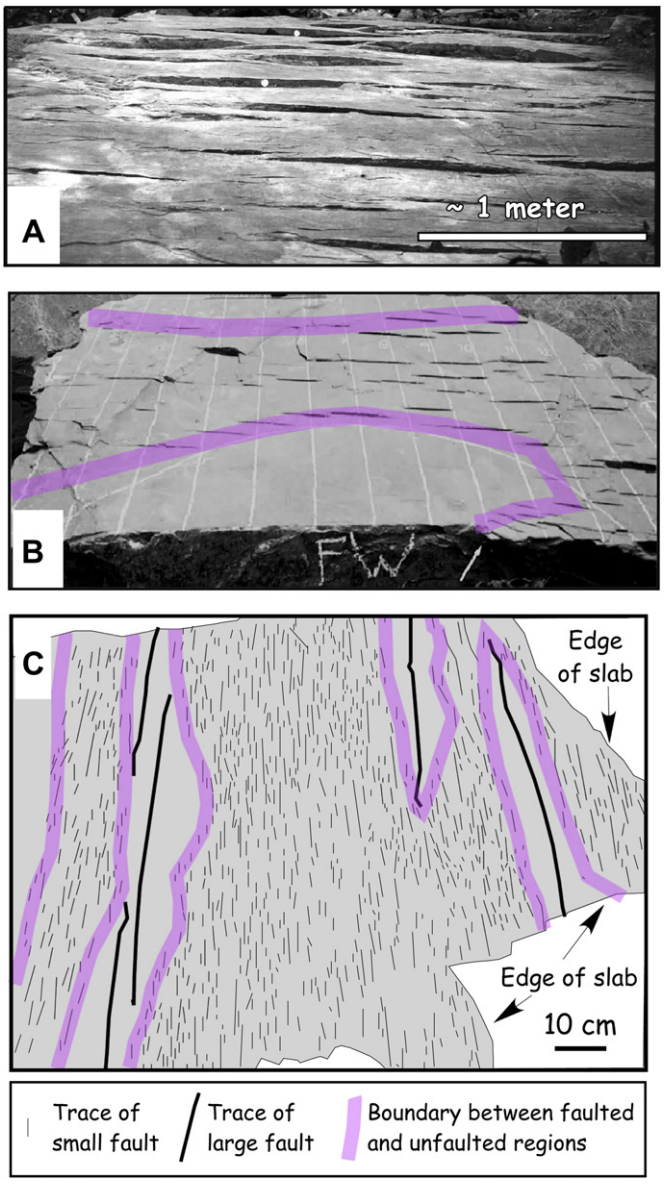

Fig. 1. Fault domains and fault-domain boundaries from the Solite Quarry in the Danville rift basin, Virginia. (A) Photograph of exhumed bedding surface cut by numerous normal faults. The bedding surface dips away and the faults dip toward the viewer. (B) Photo of slab of rock. The front and rear are bounded by relatively large slickensided fault surfaces. The top surface of the slab is a bedding surface offset by numerous small faults, which are absent in the vicinity of the larger faults. These regions without faults are interpreted as stress-reduction zones associated with the slab-bounding faults. The edges of the stress-reduction zones are a type of fault-domain boundary. The white chalk lines are 5 cm apart. (C) Sketch of faults offsetting a bedding surface from a quarried slab. Note that the population of small faults is ubiquitous except in the stress-reduction zones of the larger faults. (B) and (C) modified from Ackermann and Schlische (1997).

of E- and W-dipping faults. The Suez rift (Fig. 2B) has three fault domains (e.g., Patton et al., 1994). In the north (cross-section A–A′), the major faults dip to the NE. In the central region (cross-sections C–C′ and D–D′), the major normal faults dip to the SW. In the south (cross-sections F–F′ and G–G′), major normal faults dip to the NE. Fault-domain boundaries that are parallel to the normal faults shift location within the rift basin; they are located near the edges of the rift basin, and the shifts consist of fault-oblique domain boundaries. The fault-parallel domain boundaries exhibit a graben geometry (cross-sections AA′, D–D′, F–F′, and G–G′). At fault-oblique domain boundaries (cross-sections B–B′, C–C′ and E–E′), major normal faults with both dip directions are present, producing relatively wide grabens. In the Basin and Range province, published fault-domain boundaries are orthogonal, oblique, and parallel to the strike of normal faults (Stewart, 1980; Faulds and Varga, 1998).

Conceptual models of fault-domain boundaries are described in the literature (Fig. 3) and in structural-geology textbooks (e.g., van der Pluijm and Marshak, 2004). In some models, fault-domain boundaries are strike-slip or oblique-slip fault zones whose orientations are controlled by pre-existing zone of weaknesses (e.g., Fig. 3A; Versfelt and Rosendahl, 1989; Ebinger, 1989). In other models, fault-domain boundaries are discrete strike-slip or oblique-slip faults that parallel the extension direction (e.g., Fig. 3B and C; Bally, 1982; Angelier and Bergerat, 1983; Gibbs, 1984; Lister et al., 1986). In the models in Fig. 3D, fault-domain boundaries are zones of folding among the overlapping fault tips between adjacent fault domains (Faulds and Varga, 1998). The folds include synclines and anticlines, and the fault-domain boundaries are parallel [Fig. 3D(1)], oblique [Fig. 3D(2 and 3)], and perpendicular [Fig. 3D(4 and 5)] to the extension direction (i.e., perpendicular, oblique, and parallel to the normal faults).

Are these conceptual models realistic? Do fault-domain boundaries require the presence of pre-existing zones of weaknesses? Do fault-domain boundaries provide independent evidence of the extension direction? What structural features characterize fault-domain boundaries? How and why do fault domains and their boundaries develop? In this paper, we use scaled experimental models of orthogonal and oblique extension with wet clay and dry sand as the modeling materials to address these questions. We integrate the results of the experimental modeling with published concepts of stress-reduction zones around normal faults (e.g., Price and Cosgrove, 1990; Hodgkinson et al., 1996; Ackermann and Schlische, 1997) and near- and far-field interaction of faults in a growing population (e.g., Cowie et al., 1993, 1995; Gupta and Scholz, 2000) to show that fault domains are self-organized populations of normal faults and that some fault-domain boundaries are interference structures that develop where fault domains intersect. Our work shows that neither fault domains nor fault-domain boundaries require the presence of pre-existing zones of weakness. Also, the number of fault domains and the orientation of fault-domain boundaries are randomly controlled by the initial nucleation of faults within the extensional system.

2. Scaling, modeling materials, and experimental setup

2.1. Scaling and modeling materials

Cloos (1929, 1930) pioneered the use of scaled experimental models to simulate extensional deformation. He devised many of the experimental designs still widely used today. He also recognized the importance of scaling: "True simulation of [natural structures] and their formation is hindered by the size and time relations…. When we reduce the [structure] by a factor of 50,000, we have to choose a material which is 50,000 times less strong than [natural rocks]." Hubbert (1937) later quantified the various parameters needed to construct properly scaled physical models. In particular, experimental models must share geometric, kinematic, and dynamic similarity with the natural prototype.

Upper-crustal rocks increase in strength with depth and obey the Mohr–Coulomb criterion for failure (e.g., Byerlee, 1978),

$$\sigma_s = C_0 + (\mu\sigma_n) = C_0 + [(\tan\phi)\sigma_n] \quad (1)$$

where σ_s and σ_n are the shear and normal stress, respectively, on the potential fault, C_0 is the cohesive strength, μ is the coefficient of internal friction, and ϕ is the angle of internal friction. The latter determines the angle between the fault surfaces and the principal stresses. For natural rocks, ϕ ranges from 29° to 40° (Handin, 1966;

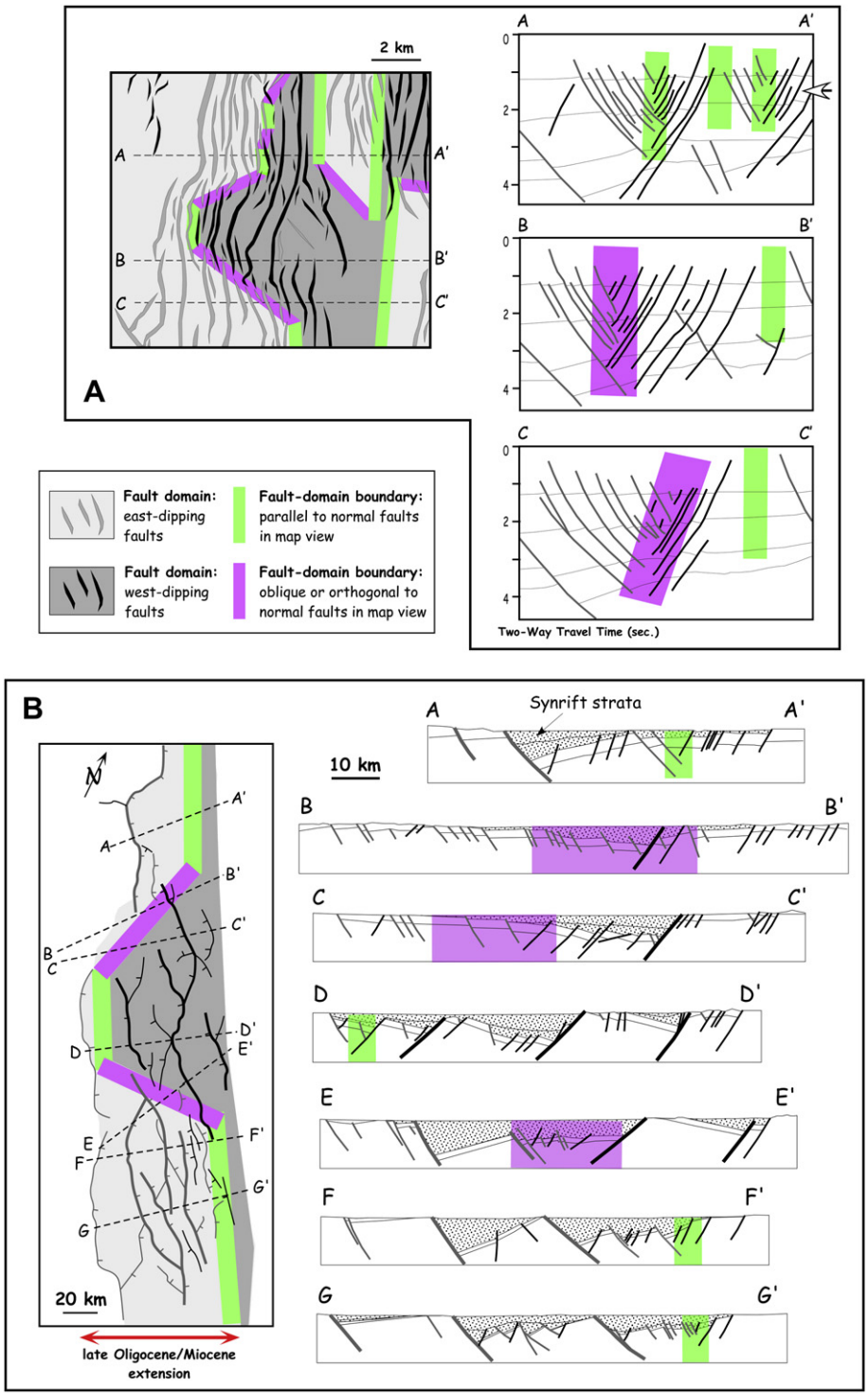

Fig. 2. Geologic examples of fault domains and fault-domain boundaries. (A) Fault-trace map (arrow shows mapped horizon) and line drawings of seismic-reflection profiles showing normal faults from the Funan field, Pattani rift basin, Gulf of Thailand. Modified from Kornsawan and Morley (2002). The profiles are displayed without vertical exaggeration assuming a velocity of 3 km s^{-1}. (B) Fault-trace map and cross-sections from the Suez rift basin, Egypt (from Patton et al., 1994). Our interpretation of the geometry of the fault-domain boundaries is based on the map of Patton et al. (1994) and the results of experimental modeling (Figs. 5 and 6).

Byerlee, 1978). Geometric similarity requires that ϕ be similar for natural rocks and modeling materials. C_0 for intact sedimentary rocks is <20 MPa (Handin, 1966) and is considerably less for highly fractured rocks (e.g., Byerlee, 1978; Brace and Kohlstedt, 1980). Dynamic similarity requires that

$$C_0^* = \rho^* g^* L^* \tag{2}$$

where C_0, ρ^*, g^*, and L^* are the model-to-prototype ratios for cohesive strength, density, gravitational acceleration, and length (e.g., Hubbert, 1937; Weijermars et al., 1993; Vendeville et al., 1995; Withjack and Callaway, 2000).

Both wet clay and dry sand obey the Mohr–Coulomb criterion for failure and have mechanical properties that satisfy the conditions for geometric and dynamic similarity (e.g., Richard and

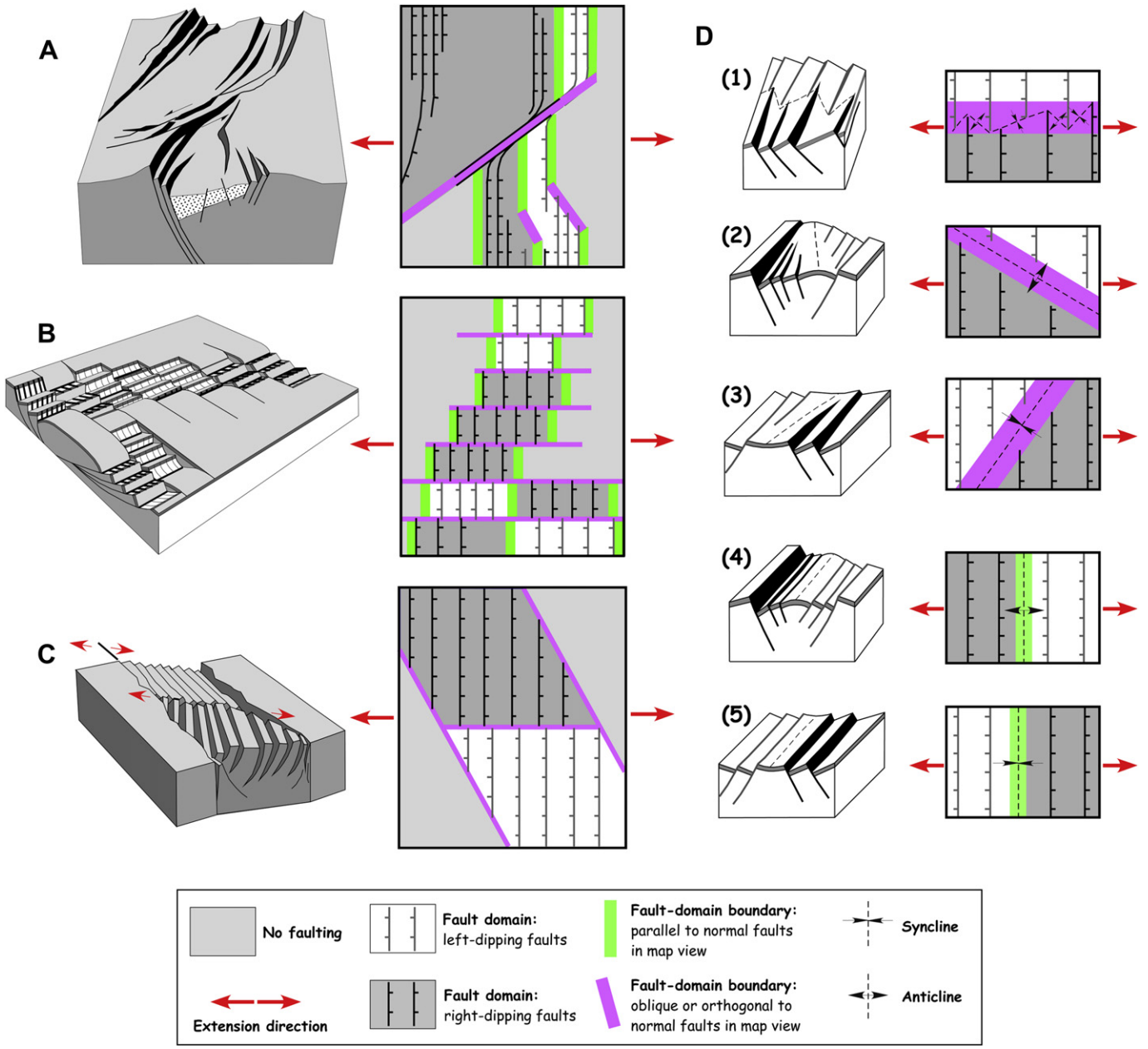

Fig. 3. Block-diagrams and map views of conceptual models of fault-domain boundaries (referred to as transfer zones or accommodation zones in the literature). (A) Discrete oblique-slip fault parallel to pre-existing zone of weakness. Modified from Ebinger (1989). (B) Discrete faults perpendicular to strike of normal faults and rift zone and parallel to extension direction. Modified from Lister et al. (1986). (C) Discrete fault parallel to extension direction and oblique to rift zone. Modified from Angelier and Bergerat (1983) and McClay and White (1995). (D) Broad zone of deformation (folding among overlapping fault tips). (1) Alternating synclines and anticlines in fault-domain boundary orthogonal to strike of normal faults. (2) Anticline oblique to strike of faults that dip toward one another. (3) Syncline oblique to strike of faults that dip away from one another. (4) Anticline parallel to strike of faults that dip toward one another. (5) Syncline parallel to strike of normal faults that dip away from one another. Modified from Faulds and Varga (1998).

Krantz, 1991; Vendeville et al., 1995; Withjack and Callaway, 2000; Eisenstadt and Sims, 2005; Withjack and Schlische, 2006; Schreurs et al., 2006; Withjack et al., 2007). The angles of internal friction (30° for wet clay, 26° for dry sand) are similar to natural rocks. C_0 for wet clay is ~50 Pa, and is considerably less for dry sand. In our models, C_0^* is $\sim 10^{-5}$ (assuming a cohesion of 5 MPa for natural rocks), ρ^* is ~0.6 (both wet clay and dry sand have the same density, 1600 kg m^{-3} compared to ~2600 kg m^{-3} for upper-crustal rocks), and $g^* = 1$. Consequently, equation (2) requires that L^* is $\sim 10^{-5}$. Thus, centimeter-scale structures in our models are equivalent to kilometer-scale structures in nature.

The dry sand in our models is composed of quartz grains with diameters of less than 0.5 mm. The wet clay in our models is composed predominantly of water (~40% by weight) and kaolinite particles (less than 0.005 mm in diameter). The wet clay and dry sand have different deformational styles because their ductilities differ. Ductility is the capacity for distributed deformation at the scale of observation (Rutter, 1986). Both wet clay and dry sand deform by faulting (e.g., Maltman, 1987; Richard and Krantz, 1991; Withjack and Callaway, 2000). Because of its low ductility, deformation in dry sand is localized on a few major faults, even at small strains. Because of its much higher ductility, deformation in wet

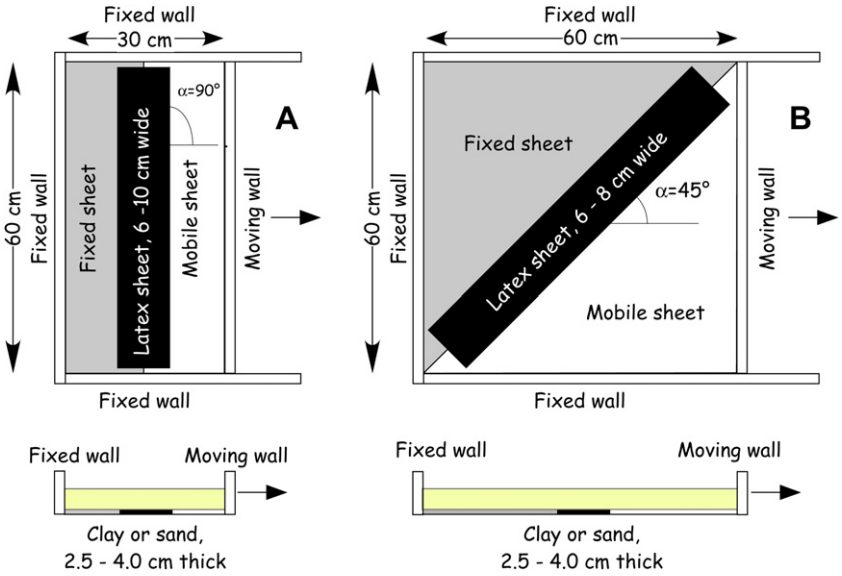

Fig. 4. Sketch of experimental modeling apparatus and boundary conditions for (A) orthogonal extension ($\alpha = 90°$) and (B) oblique extension ($\alpha = 45°$).

clay is distributed on numerous minor to major faults. With increasing strain, however, most deformation becomes localized on a few major faults.

2.2. Experimental setup

Two metal sheets form the base of the experimental apparatus (Fig. 4). One sheet is attached to a fixed wall, and the other sheet is attached to a movable wall. A thin latex sheet, attached to both sheets, straddles the boundary between the metal sheets. A layer of wet clay or dry sand covers the latex sheet and the exposed metal sheets. As the movable wall and attached metal sheet move outward (at a constant rate), the latex sheet and the overlying clay or sand layer deforms. In orthogonal deformation, the displacement direction is perpendicular to the edge of the rubber sheet, and the latex sheet undergoes only stretching (Fig. 4A). If the displacement direction is oblique to the edge of the latex sheet, the deformation involves both stretching and shearing. The angle between the displacement direction and the rift zone (α as defined in Withjack and Jamison, 1986) varied from 45° to 90° in 15° increments (Fig. 4B).

We photographed the top surface of the models at regular displacement increments to record the surface deformation through time. Low-angle lighting enhanced the fault scarps, producing bright scarps that dip toward the light source and dark scarps that dip away from the light source. Folds appear as gradual changes in illumination of the model surface. We also vertically sectioned several of the clay and sand models to document the deformation within the models. To test the robustness of the modeling results, we ran similar models varying: (1) the initial width of the rubber sheet (from 6 to 10 cm); (2) the thickness of the clay layer (2.5 and 4 cm); (3) the displacement rate of the movable wall (1 cm h^{-1} to 36 cm h^{-1}); and (4) the presence of growth layers. Although the number and shape of the fault domains and the number and orientation of the fault-domain boundaries varied during these experiments, even for multiple runs of experiments with identical boundary conditions, the key modeling results were consistent.

3. Experimental clay and sand models of extension

In all models (Figs. 5–11), normal faults form in the clay and sand above the stretched latex sheet. The normal faults dip moderately either toward or away from the moving wall. The largest faults cut through the entire model, the smaller faults extend from either the top or bottom surface and tip out within the model, and the smallest faults have both tip lines within the model. The number of normal faults increases and their average displacement decreases toward the bottom of the model. The average strike of the normal faults is perpendicular to the extension direction, which is parallel to the displacement direction for orthogonal extension (Figs. 5–7 and 10) and oblique to the displacement direction for oblique extension (Figs. 8, 9 and 11). Like natural faults, the faults in the models exhibit decreasing displacement toward the fault tips and irregular fault traces resulting from hard linkage of non-coplanar fault segments. In the clay models, folds include monoclinal relay ramps between offset fault segments and fault-displacement folds with hinge lines subperpendicular to the strike of the faults (hanging-wall synclines and footwall anticlines at local displacement maxima, hanging-wall anticlines and footwall synclines at local displacement minima). Withjack and Jamison (1986), Clifton et al. (2000), Clifton and Schlische (2001), Ackermann et al. (2001), and Bellahsen et al. (2003) describe in detail the geometry and evolution of faults and fault populations in clay models for the same boundary conditions used in this study.

In all models, the geometry of bedding varies within the deformed zone (see cross-sections in Figs. 6, 7 and 10). The basal boundary condition forces bedding to be flat at the bottom of the models. Near the edges of the deformed zone, the bedding dips gently toward the center of the deformed zone, reflecting the transition from undeformed clay or sand to thinned and extended clay or sand above the latex sheet. In the center of the deformed zone, the bedding dips in a direction opposite to that of the adjacent normal faults. Bedding dips are also apparent in map view. For example, Fig. 9C shows that the clay surface in the area of left-dipping faults is brighter than in the adjacent areas with right-dipping faults. With the light source positioned on the right side of the model, the brighter clay surface dips toward the light source, opposite to the dip direction of the faults.

3.1. Geometry of fault domains

Fault domains are present in all models, but their number and arrangement are highly variable, even for models with similar or

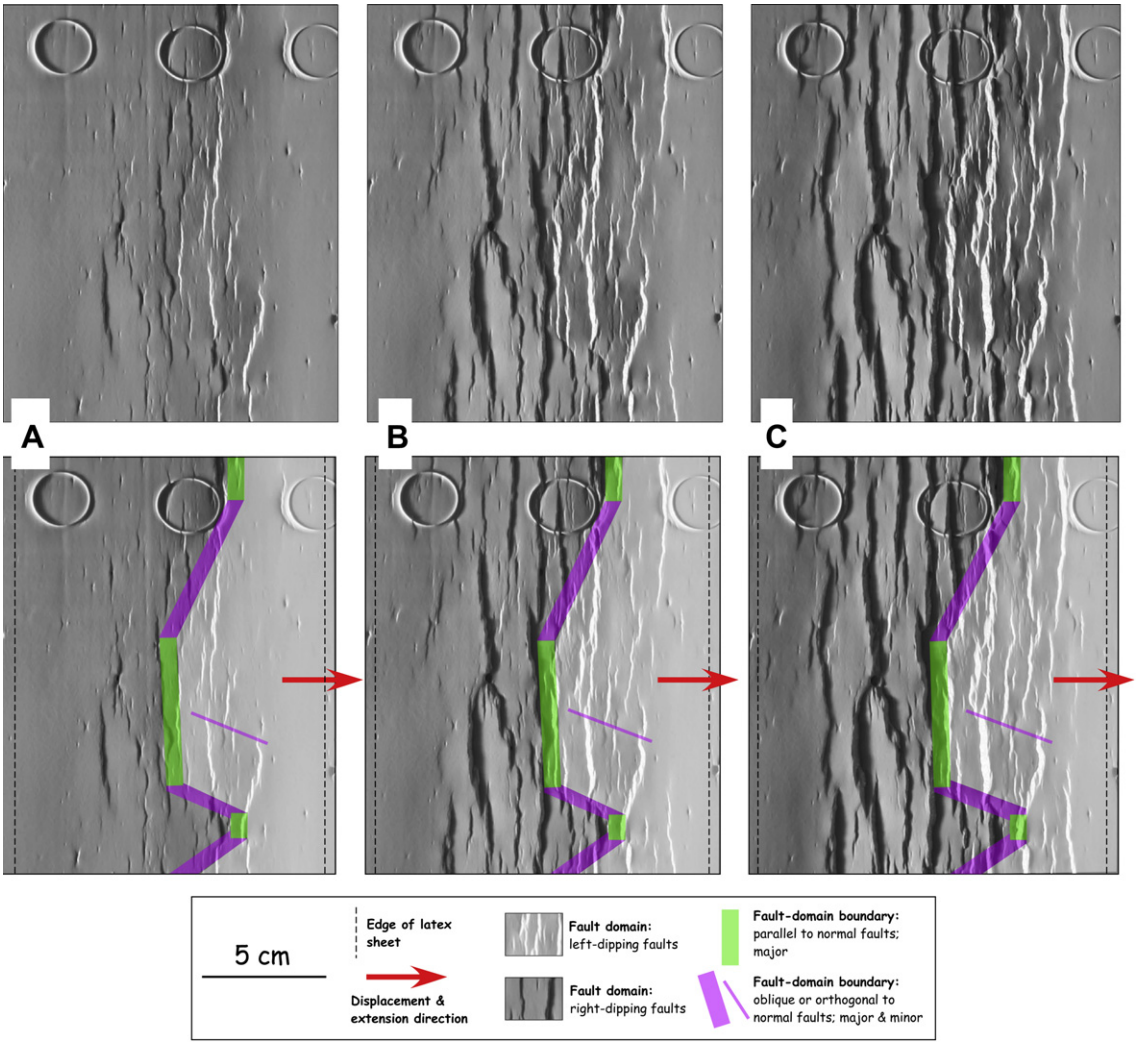

Fig. 5. Photos of top surface of clay model of orthogonal extension (top row, uninterpreted; bottom row, interpreted). Fault scarps appear as bright features dipping toward light source on left, and dark features dipping away from light source. Latex sheet is initially 10-cm wide, clay thickness is 2.6 cm, and displacement rate is 8 cm h^{-1}. Photos taken at: (A) 2.5 cm, (B) 3.5 cm, and (C) 4.5 cm of displacement (25%, 35%, 45% strain, respectively).

identical boundary conditions. For example, the oblique-extension models with clay in Fig. 8 have two main fault domains at the top surface. In contrast, the oblique-extension model with clay in Fig. 11A has one very large fault domain and three small subdomains at the top surface. The oblique-extension model with sand in Fig. 11B has three fault domains at the top surface. In many models, the fault domains are arranged symmetrically relative to the axis of the deformed zone. Faults on the left side generally dip to the right, and those on the right side generally dip to the left (Figs. 5–8B). In other models, the fault domains extend across most, if not all, of the deformed zone. For example, in the oblique-extension models with clay (Fig. 8A and C), most of the faults on one end of the deformed zone dip to the left, whereas most of the faults on the opposite end dip to the right. In all models, the number of fault domains, like the number of faults, increases with depth. In the orthogonal-extension model with clay in Fig. 7, two fault domains exist at the top surface of the model. Cross-sections show that these same fault domains, as well as several small subdomains, exist at depth. For example, a small subdomain of left-dipping faults exists near the left side of the deformed zone in cross-section 66, and a small subdomain of right-dipping faults exists near the right side of the deformed zone in cross-section 0.

3.2. Geometry of fault-domain boundaries

In map view, fault-domain boundaries are either parallel or oblique to the normal faults in the adjacent fault domains. In some models (e.g., orthogonal extension with clay, Fig. 6), the total length of the fault-parallel and fault-oblique boundaries is approximately equal. In other models, either the fault-parallel or fault-oblique boundaries predominate. For example, in the orthogonal-extension model with sand (Fig. 10), the fault-parallel boundaries predominate, whereas in the oblique-extension model with sand (Fig. 11B), the fault-oblique boundaries predominate. Although the trend of some fault-domain boundaries (~20%) is subparallel to the extension direction (i.e., subperpendicular to the normal faults in the adjacent fault domains), the trend of most fault-domain boundaries (~80%) is oblique or perpendicular to the extension direction (i.e., oblique or parallel to the normal faults in the adjacent fault domains). In map view, fault-parallel boundaries contain few, if any, fault terminations, whereas fault-oblique boundaries contain numerous fault terminations. Fault-oblique boundaries also contain a large number of faults whose lengths are less than the average length of faults in the domains themselves (see especially the fault-oblique boundaries in Fig. 5C and the fault-oblique boundary in Fig. 8D). Most fault-parallel and fault-oblique

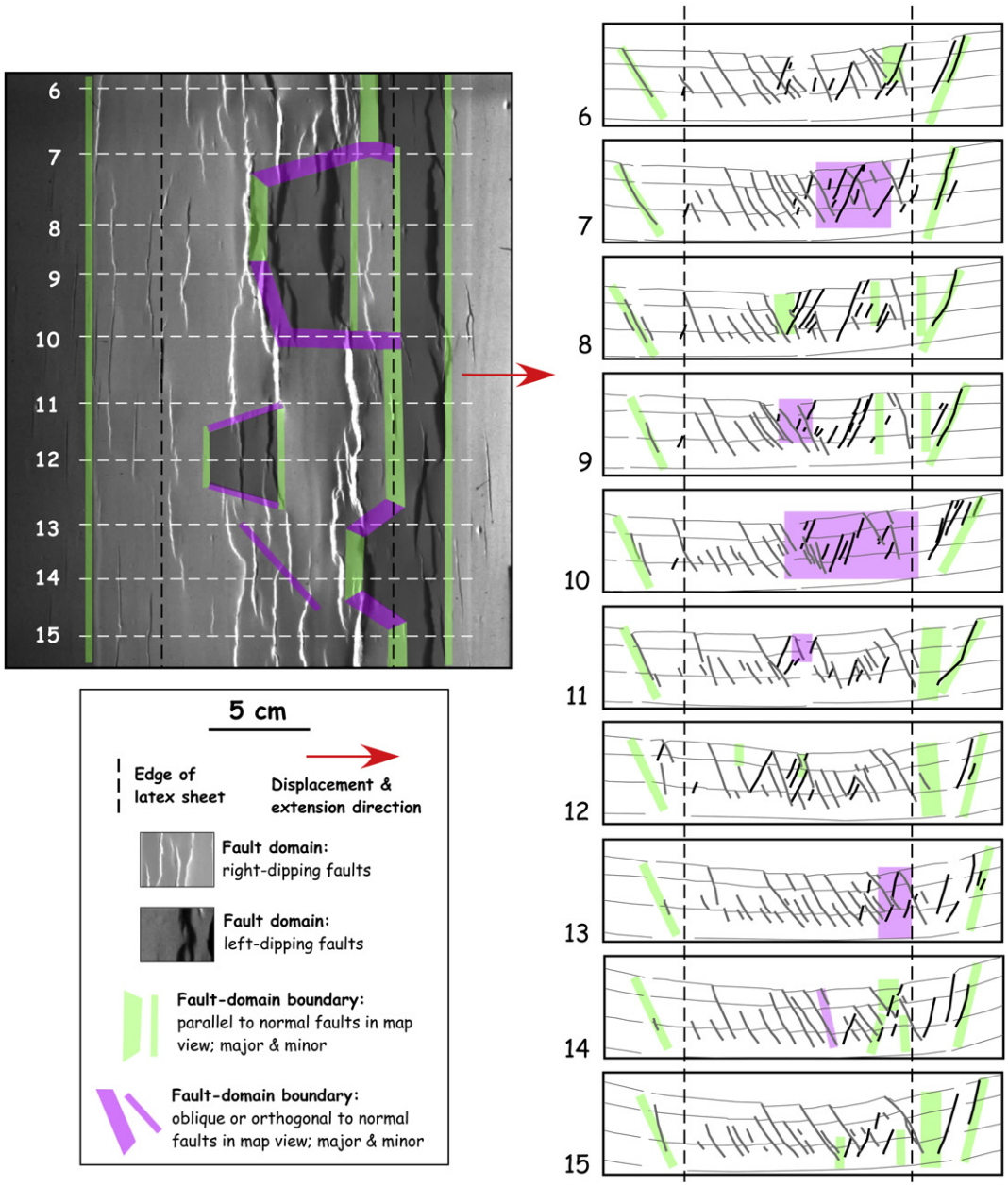

Fig. 6. Photo of top surface and line drawings of cross-sections through clay model of orthogonal extension showing fault domains and fault-domain boundaries. Bright faults dip toward light source on right, and dark faults dip away from light source. Thin gray lines in cross-sections are horizons in the layered clay model. Thick gray and black lines are right- and left-dipping faults, respectively. Latex sheet is initially 9-cm wide, clay thickness is 3.9 cm, and displacement rate is 1 cm h^{-1}. Photo taken at 2.5 cm of displacement (27.8% strain).

boundaries link up along strike. Most intersection angles are obtuse (~60%), with ~20% each for orthogonal and acute angles. The greatest percentage (34%) of orthogonal intersections (and, consequently, fault-domain boundaries that parallel the extension direction) is in the clay models of oblique extension, but obtuse intersections still predominate (>40%).

In dip sections (i.e., cross-sections oriented perpendicular to the strike of the normal faults), most fault-parallel and fault-oblique boundaries have either a graben or a horst geometry (e.g., cross-sections 15 and 30 in Fig. 7, cross-sections 12 and 15 in Fig. 10). Commonly, these graben and horst geometries are complex, composed of numerous, interacting faults of opposing dip (e.g., the fault-parallel and fault-oblique boundaries in Figs. 7 and 10). Within these fault-domain boundaries, some faults lose displacement near faults of opposing dip (Fig. 10, box in cross-section 15), and some faults are offset by faults of opposing dip (Fig. 7, box in cross-section 66; Fig. 10, boxes in cross-sections 15 and 19). As discussed by Ferrill et al. (2000), alternating sequential slip on crossing normal faults can produce complex fault patterns. Folds are also common within fault-domain boundaries. For example, in the dip sections in Fig. 7, bedding defines an anticline resulting from the reversal of bedding dip across the fault-domain boundaries, not shortening.

Although most fault-domain boundaries separate fault domains with opposing fault-dip directions, some fault-domain boundaries separate fault domains with the same fault-dip direction. For example, the minor fault-oblique boundary in Fig. 6 (cross-section 14) separates faults with the same dip direction and, hence, consists of tilted fault blocks in cross-section. The spacing and displacement of the faults differ in the two adjacent fault domains, and many faults terminate within the fault-domain boundary. Some fault-domain boundaries separate highly faulted versus relatively unfaulted parts of the model (e.g., the two minor domain

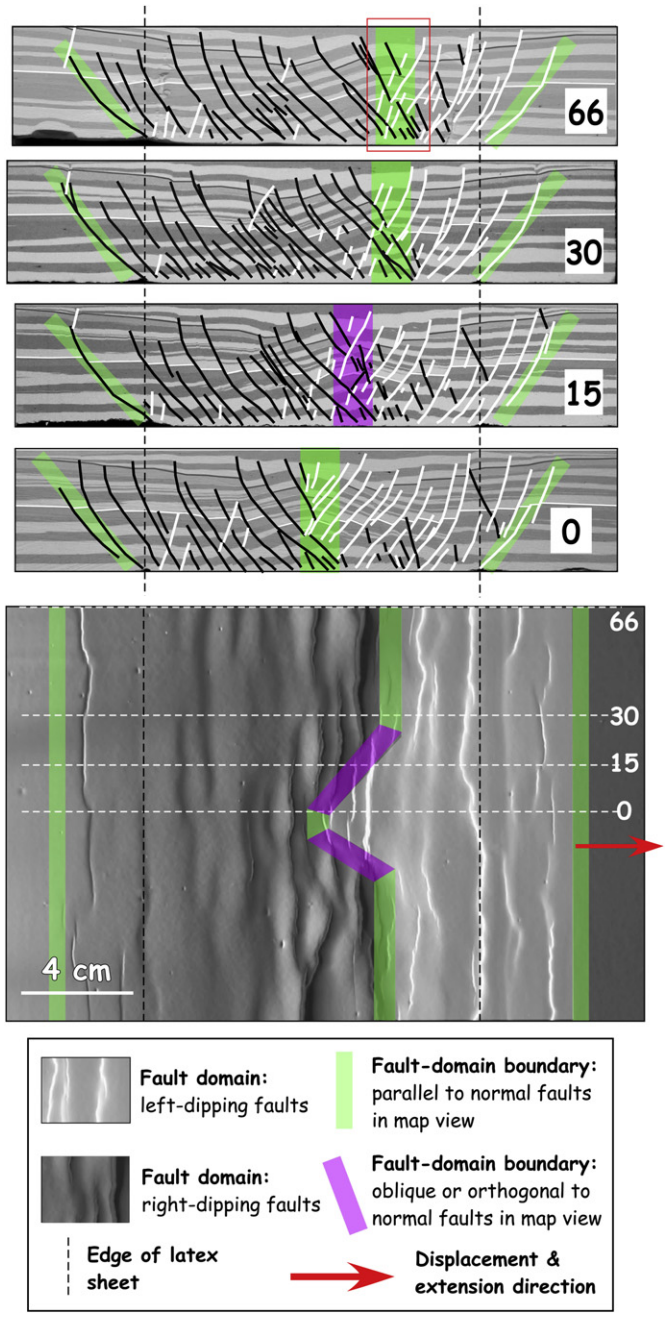

Fig. 7. Photo of top surface and cross-sections through clay model of orthogonal extension showing fault domains and fault-domain boundaries. Bright faults dip toward light source on left, and dark faults dip away from light source. Top four layers in cross-sections are growth layers added during deformation. Thin gray line is base of growth layers. Thick black and white lines are right- and left-dipping faults, respectively. Latex sheet is initially 8-cm wide, clay thickness is 4.0 cm, and displacement rate is 4 cm h^{-1}. Photo taken at 4 cm of displacement (50% strain). The box in cross-section 66 shows white faults offset by black faults within a fault-domain boundary.

boundaries in Fig. 8C and the edges of the deformed zone in Figs. 10 and 11B). The fault-domain boundaries at the edges of the deformed zone are well developed in the sand models, whereas they are poorly developed in the clay models.

3.3. Evolution of fault domains and fault-domain boundaries

The experimental models show the temporal evolution of the fault domains and their boundaries (Figs. 5 and 9). Initially, numerous small normal faults form, nucleating at impurities (e.g., air bubbles) within the clay (e.g., Fig. 9A, 1.75 cm; Fig. 9B, 2.2 cm). These small faults dip in both directions, and no obvious fault domains exist. As strain increases, many of these small faults become inactive. Others, however, remain active, growing through tip propagation and linkage (Fig. 9A, 2.0 cm; Fig. 9B, 2.8 cm). Generally, the active faults have the same polarity as adjacent active faults. New faults also form with the same polarity as the active faults. As strain increases, this process leads to the formation of well-defined fault domains and fault-domain boundaries (Figs. 8D and 9A, 3.0 cm; Fig. 9B, 3.4 cm and 4.0 cm). In both the clay and sand models, the fault-oblique domain boundaries consist of the overlapping tips of faults from the adjacent fault domains. In the clay models, the fault-oblique boundaries also contain a number of small faults, and the clay surface is warped into a complex series of low-amplitude anticlines and synclines (Figs. 8D and 9C). With increasing strain, the fault-domain boundaries in the clay models become narrower and better defined (Figs. 5, 8D and 9). Fault-parallel boundaries do not change length with increasing strain, whereas fault-oblique boundaries increase in length as strain increases.

4. Summary and discussion

4.1. Summary of modeling results

Our models show that: 1) fault domains and fault-domain boundaries form spontaneously without the presence of pre-existing zones of weakness. Their exact number, size, and arrangement vary, even in similar or identical experiments. 2) Most fault-domain boundaries separate fault domains with opposing fault-dip directions. Some fault-domain boundaries, however, separate fault domains with the same fault-dip direction; the spacing and displacement of the faults differ in the adjacent fault domains. Other fault-domain boundaries separate fault domains from unfaulted regions. 3) Fault-domain boundaries are either parallel or oblique to the normal faults in adjacent fault domains. Relatively few fault-domain boundaries trend parallel to the extension direction. 4) In map view, fault-parallel boundaries contain few, if any, fault terminations, whereas fault-oblique boundaries contain numerous fault terminations and small faults. The cross-section geometries of fault-domain boundaries include horsts, grabens, multiple horsts and grabens, and tilted fault blocks. 5) Fault-parallel boundaries commonly link along strike with fault-oblique boundaries.

Published models with similar boundary conditions have yielded similar results (e.g., Cloos, 1930; Bain and Beebe, 1954; Withjack and Jamison, 1986; Vendeville et al., 1987; Kautz and Sclater, 1988; McClay et al., 2002; Bellahsen et al., 2003), although none of these publications specifically addressed the geometry and origin of fault-domain boundaries. Fault domains and fault-domain boundaries also developed in clay and sand models with different basal boundary conditions. For example, fault domains and fault-domain boundaries developed in sand (Tron and Brun, 1991) and clay models (Schreurs et al., 2006) with a basal putty layer, rather than a basal latex sheet; they also formed in clay models with a basal latex sheet directly overlain by a putty layer (Bellahsen et al., 2003). Also, sand models simulating the secondary faulting in the rollover structure of a listric fault (Naylor et al., 1994) generated fault domains in all experiments and fault-oblique domain boundaries in about one-third of the experiments. Single fault domains developed in models with some asymmetry or heterogeneity: downslope flow of a ductile substratum (e.g., Brun et al., 1994), stretching above a dipping detachment (e.g., McClay and Ellis, 1987; Vendeville et al., 1987; McClay, 1989), non-uniform thickness of the overburden (Higgs and McClay, 1993) and strain

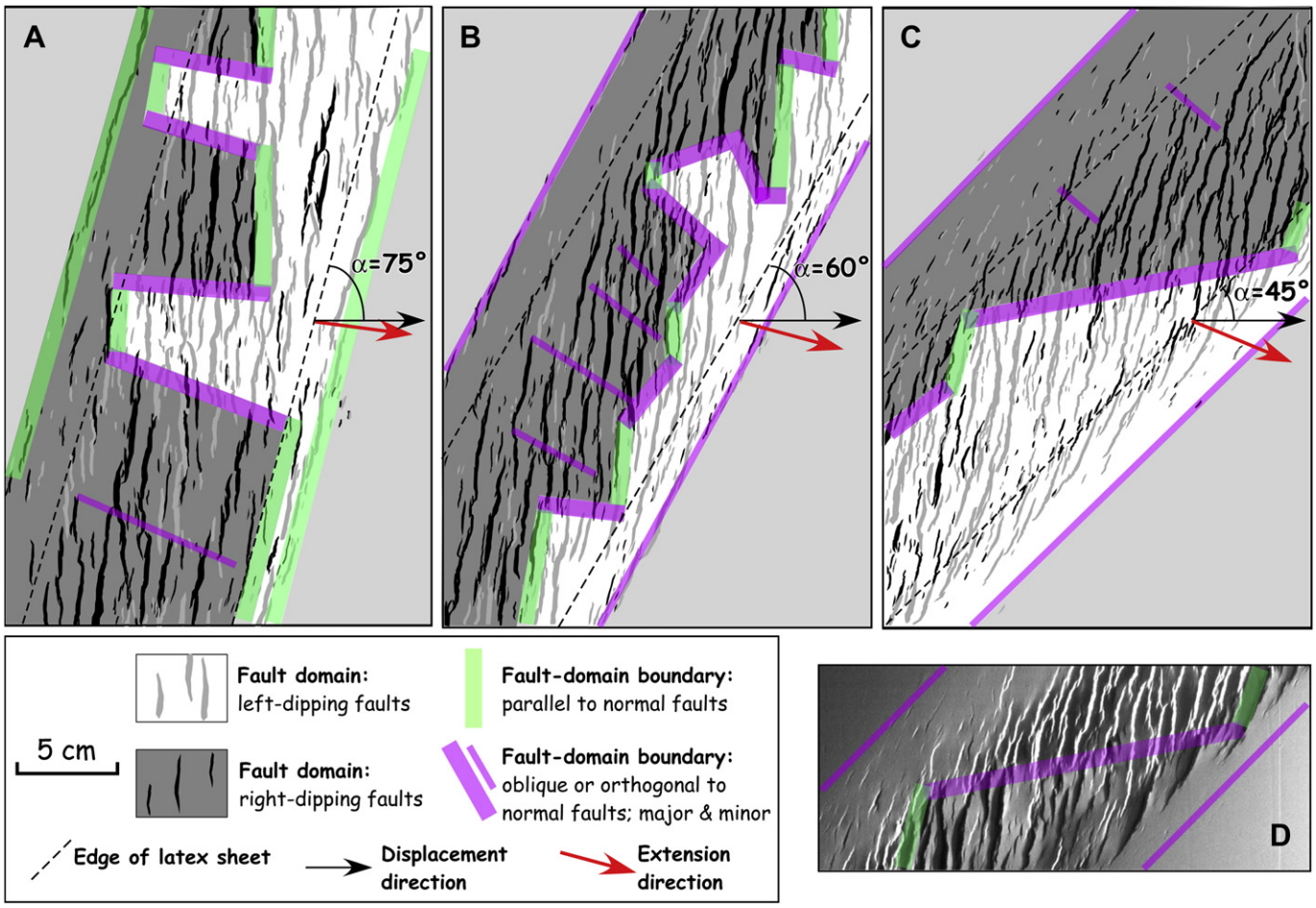

Fig. 8. Fault-trace maps of models of oblique extension (modified from Clifton et al., 2000): (A) $\alpha = 75°$, (B) $\alpha = 60°$, and (C) $\alpha = 45°$. D. Photo of top surface of oblique-extension model in (C). Latex sheet is initially 6-cm wide, clay thickness is 2.5 cm, displacement rate is 3 cm h^{-1}, and total displacement is 3.5 cm.

gradients in the latex sheet (Ishikawa and Otsuki, 1995). Our models show that single, major fault domains may develop during symmetrical, homogeneous deformation (e.g., Fig. 11A). Thus, the presence of a single natural fault domain by itself does not necessarily imply the existence of a geological asymmetry or heterogeneity such as a dipping detachment (cf. Stewart and Argent, 2000).

4.2. Conceptual model

Using our modeling results, we have classified fault-domain boundaries based on map-view and cross-section geometries (Fig. 12). In map view, fault-domain boundaries have two distinct end-member types: 1) boundaries that are parallel to the normal faults and not associated with fault terminations in map view, and 2) boundaries that are oblique or perpendicular to the normal faults and consist of fault terminations in map view. In cross-sections, fault-domain boundaries have either a tilted-fault-block geometry (Fig. 12A–C), a horst geometry (Fig. 12D and E), a graben geometry (Fig. 12F and G), or a hybrid geometry. As shown in Fig. 12, fault-domain boundaries with very different map-view geometries can have similar cross-section geometries in dip sections. For example, fault-parallel boundaries can have either a horst (Fig. 12D) or a graben geometry (Fig. 12F), and fault-oblique boundaries can have either a horst (Fig. 12E) or a graben geometry (Fig. 12G).

Linked fault-domain boundaries have obtuse, orthogonal, or acute intersection angles (Fig. 12H–J). If the intersection angle is obtuse, then linked fault-parallel and fault-oblique boundaries have similar geometries in cross-section (e.g., both have graben geometries or both have horst geometries) (Fig. 12H). If the intersection angle is acute, then linked fault-parallel and fault-oblique boundaries have different geometries in cross-section (e.g., one has a graben geometry and the other has a horst geometry) (Fig. 12J). If the intersection angle is ~90°, then fault-oblique boundaries have a complex geometry consisting of alternating horsts and grabens (Fig. 12I).

What do our modeling results imply about the conceptual models in Fig. 3? Our models suggest that fault-domain boundaries can form spontaneously without the need for pre-existing zones of weakness (cf. Fig. 3A). However, our models do not rule out the possibility that pre-existing zones of weakness may influence the development of fault-domain boundaries in nature. Our models also show that fault-domain boundaries are not proxies for the extension direction, contrary to the conceptual models in Fig. 3B (Lister et al., 1986) and C (Angelier and Bergerat, 1983). Finally, our models suggest that fault-domain boundaries are diffuse zones of deformation consisting of fault terminations, small faults, and folds, contrary to the conceptual models in Fig. 3B (Lister et al., 1986) and C (Angelier and Bergerat, 1983). The fault-domain boundaries in our models most closely resemble the wide zones of distributed deformation in the conceptual models in Fig. 3D (Faulds and Varga, 1998). Fig. 3D(2) has a fault-oblique geometry in map view and a graben geometry in cross-section like Fig. 12G. Fig. 3D(3) has a fault-oblique geometry in map view and a horst geometry in cross-section like Fig. 12E. Fig. 3D(4) has a fault-parallel geometry in map view and a graben geometry in cross-section like Fig. 12F. Fig. 3D(5) has a fault-parallel geometry in map view and a horst geometry in cross-section like Fig. 12D.

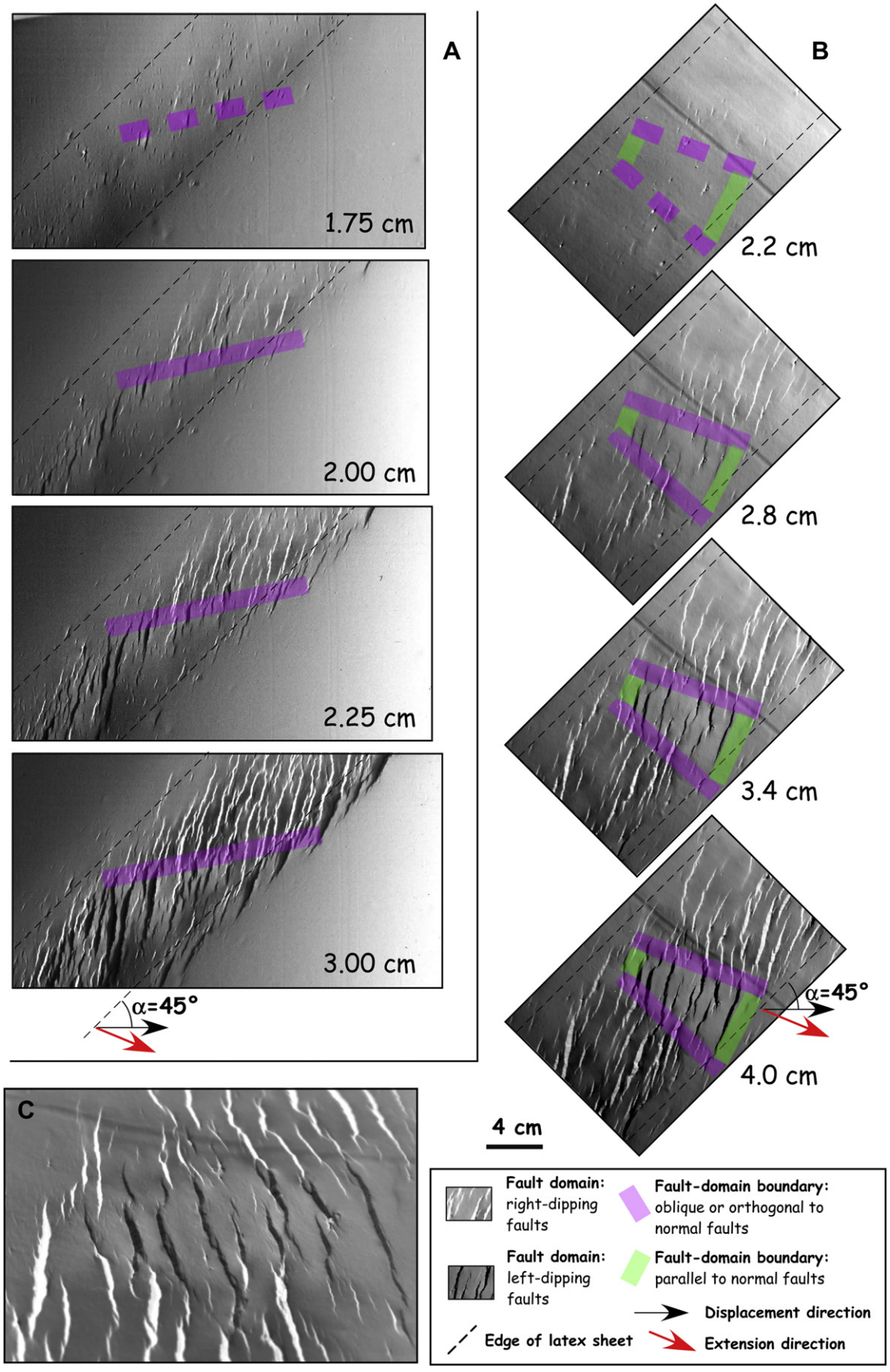

Fig. 9. (A). Evolution of fault domains and fault-domain boundary for oblique-extension model ($\alpha = 45°$) with clay in Fig. 8C. (B) Evolution of fault domains and fault-domain boundaries for oblique-extension model ($\alpha = 45°$) with clay in Fig. 11A. (C) Close-up photo of clay surface in (B) (4 cm).

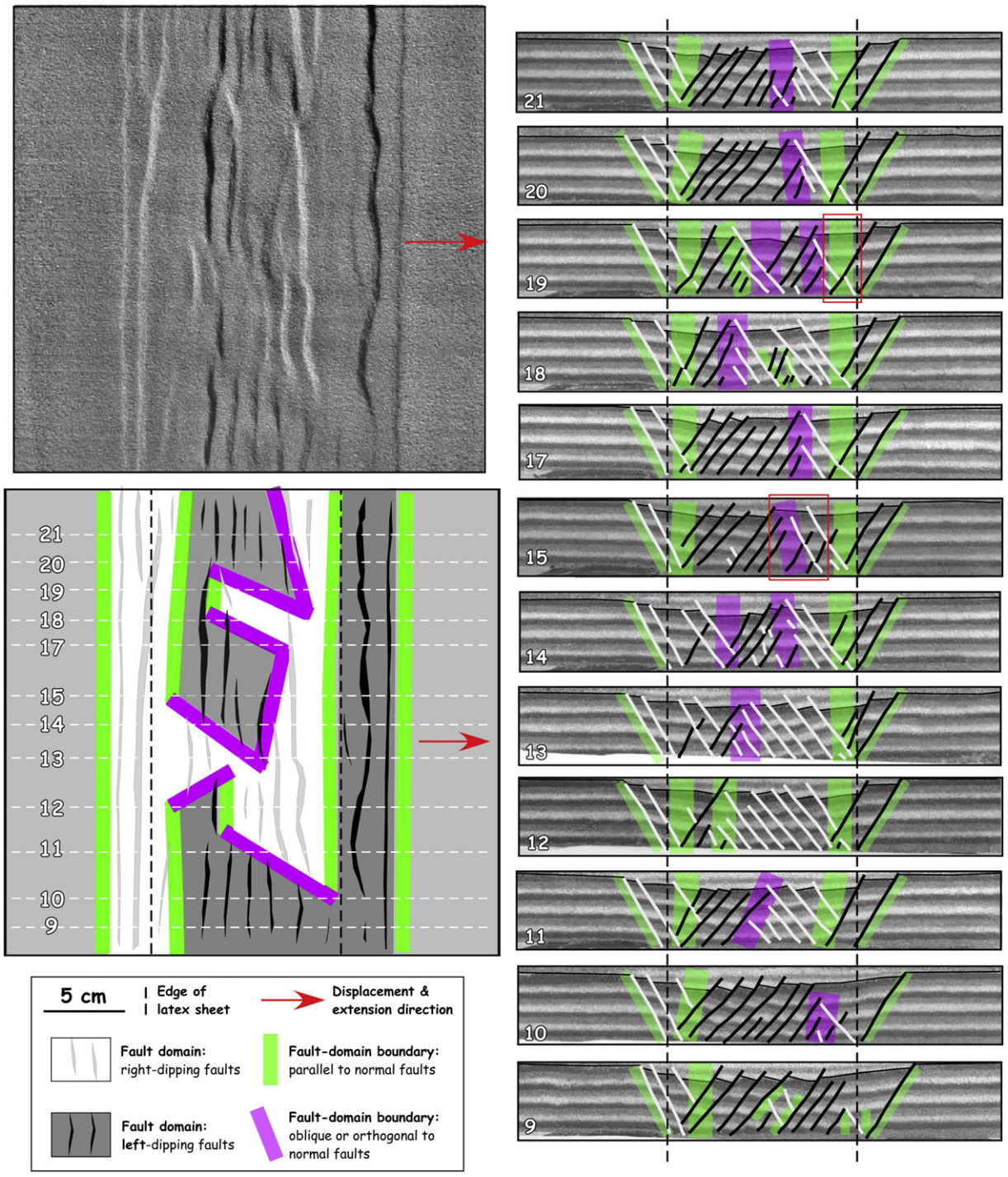

Fig. 10. Photo (top) and fault-trace map (bottom) of top surface and cross-sections through sand model of orthogonal extension. Thin black line in cross-sections marks the bottom of the growth layers. Thick white and black lines are right- and left-dipping faults, respectively. Latex sheet is initially 8-cm wide, sand thickness is 4.0 cm, and displacement rate is 4 cm h^{-1}. Photo taken at 4.0 cm of displacement (50% strain) prior to addition of last growth layer. The box in cross-section 19 shows a white fault offset by a black fault. The box in cross-section 15 shows black faults offset by white faults and black faults losing displacement near white faults.

The fault domains and fault-domain boundaries in our models resemble the fault domains and fault-domain boundaries in the Pattani rift basin, Gulf of Thailand, and the Suez rift basin, Gulf of Suez (Fig. 2). In the Pattani rift basin, both fault-parallel and fault-oblique domain boundaries develop, separating fault domains with E- and W-dipping normal faults. In dip sections, the linked fault-parallel and fault-oblique domain boundaries have similar geometries (either horsts or grabens) and are vertical or steeply inclined. In both map view and cross-section, they are diffuse zones containing numerous fault terminations and small faults. They closely resemble the domain boundaries in Fig. 7 in both map view and cross-section. Kornsawan and Morley (2002) propose that the fault-oblique domain boundaries in the Pattani rift basin are indirectly related to pre-existing zones of weakness. Our modeling results, however, suggest that similar features can develop spontaneously without the influence of pre-existing zones of weakness. In the Suez rift basin, both fault-parallel and fault-oblique domain boundaries developed between fault domains with NE- and SW-dipping normal faults. In each fault domain, the bedding dips in a direction opposite to that of the faults. Generally, the

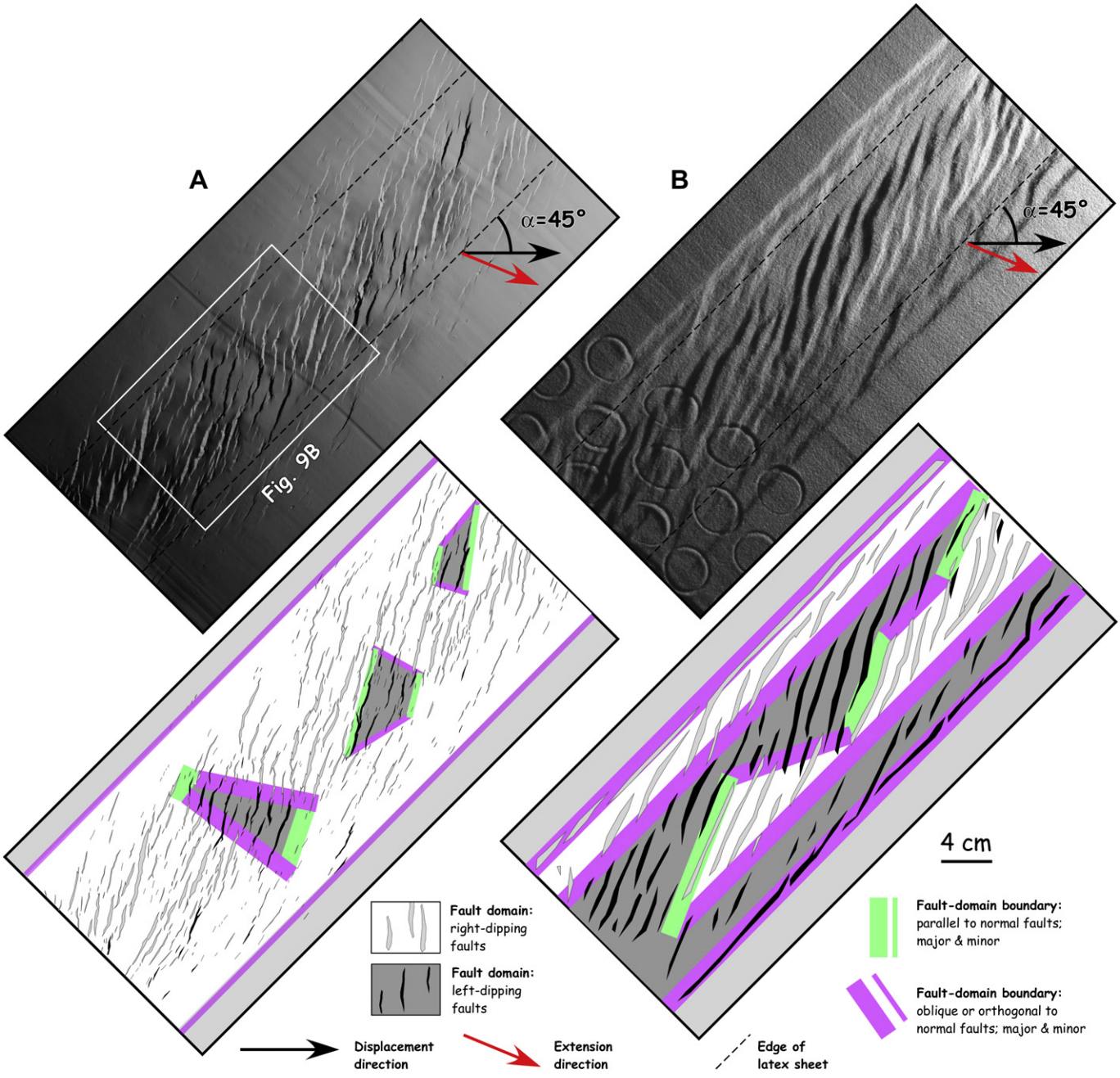

Fig. 11. Photo (top) and line drawing (bottom) of top surface of (A) clay model and (B) sand model of oblique extension ($\alpha = 45^\circ$) after 4.0 cm of displacement. Latex sheet is initially 8-cm wide, thickness of clay or sand layer is 4.0 cm, and displacement rate is 4 cm h^{-1}.

fault-domain boundaries are wide, poorly defined zones of fault terminations and small faults. Although most researchers (e.g., Moustafa, 1976, 2002; Colletta et al., 1988; Younes and McClay, 2002) relate the fault-oblique domain boundaries to pre-existing zones of weakness in the basement, our modeling results suggest that similar features are likely to develop without the presence of pre-existing zones of weakness.

4.3. Origin of fault domains and domain boundaries

To understand how fault domains develop, we consider the importance of stress-reduction zones. These are regions surrounding faults where faulting has caused a stress drop (e.g., Hodgkinson et al., 1996), such that the stress magnitude is lower than that required to produce faulting. In the Solite Quarry of the Danville rift basin (Fig. 1B and C), the stress-reduction zones around relatively large faults are marked by an absence of smaller faults, which are otherwise ubiquitous (Ackermann and Schlische, 1997). The stress-reduction zones are observed in plan view and in cross-section. According to Ackermann and Schlische (1997), the size of the stress-reduction zone is proportional to the size of the fault, a result also obtained by Gupta and Scholz (2000). Stress-reduction zones are also present in the experimental models. For example, the largest right-dipping fault in Fig. 5A has a semi-elliptical zone of fault terminations on its right side that resembles the stress-reduction zones in Fig. 1B and C.

Fig. 13 shows one possible scenario for the origin of fault domains based on a conceptual model proposed by Mandl (1987) and Price and Cosgrove (1990) and invoked by Kornsawan and Morley (2002) to explain the fault domains in Fig. 2A. Initially,

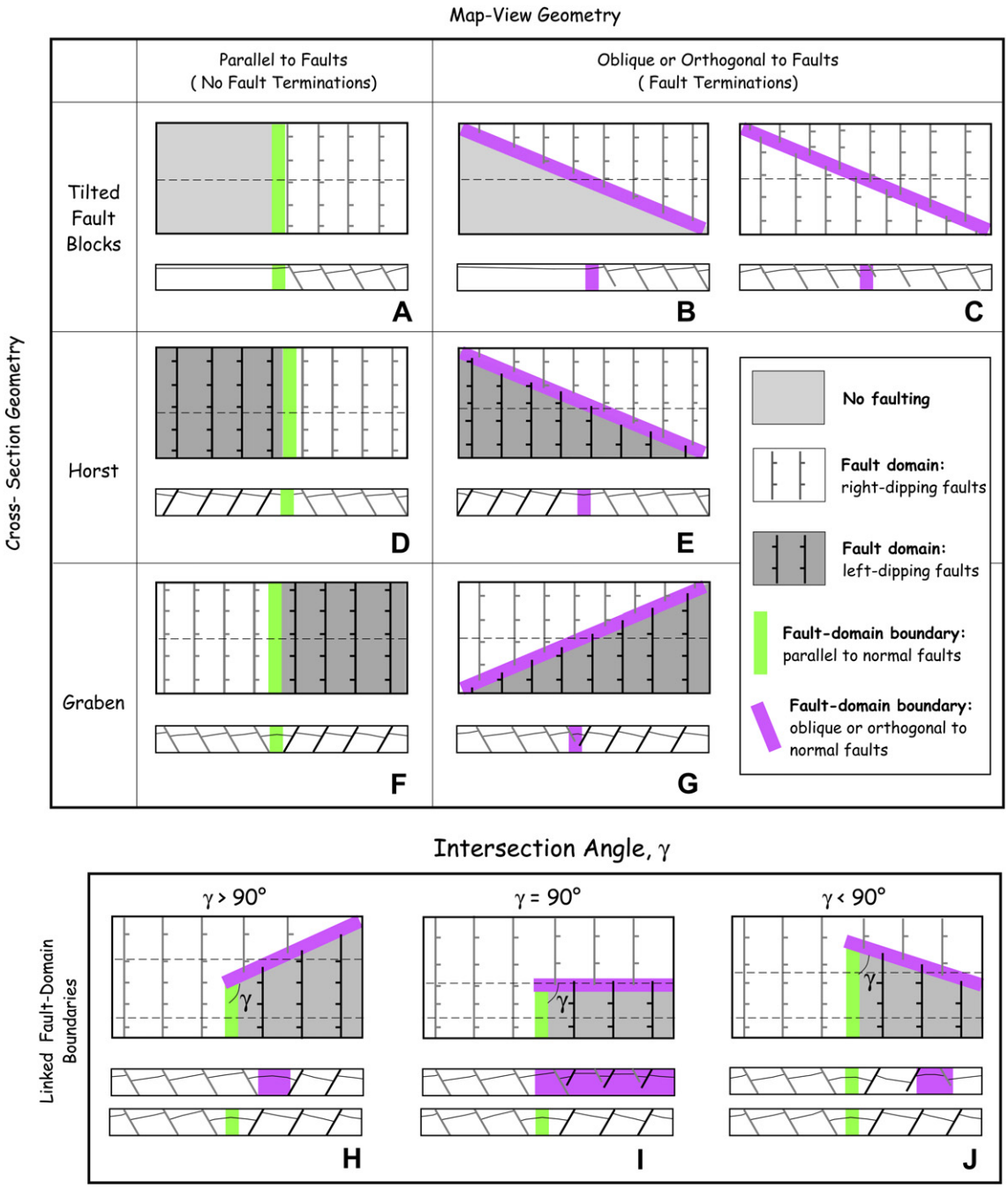

Fig. 12. (A–G) Types of fault-domain boundaries based on cross-section and map-view geometries in experimental models. Cross-section geometries include horst, graben, tilted fault block, and hybrid. Map-view geometries include fault-parallel with no fault terminations and fault-oblique to fault-orthogonal with fault terminations. (H–J) Types of linkages of fault-domain boundaries in map view and cross-section. See text for further discussion.

faults have an equal probability of dipping in either direction. In panel 1 of Fig. 13A, two faults of opposite dip are present. The fault on the left is larger than the fault on the right, perhaps because the left fault nucleated first. In panel 2, both faults have grown, but the fault on the right has reached its maximum extent because it cannot propagate into the stress-reduction zone of the larger fault. In panel 1 of Fig. 13B, two faults of similar dip are present, and the fault on the left is larger than the fault on the right. In panel 2, both faults have grown. In panel 3, both faults continue to grow because the smaller fault has not propagated into the stress-reduction zone of the larger fault. Thus, it is easier for a fault with the same dip direction as the larger fault to nucleate and grow. Our experimental models, which show the temporal development of the fault domains, corroborate this conceptual model for the origin of fault domains (e.g., Fig. 13C). Initially, normal faults with both dip directions develop. As strain increases, however, the faults dipping to the right (dark) continue to develop, whereas the faults dipping to the left (light) become inactive.

Fig. 13D is a conceptual model for the development of fault-domain boundaries. In panel 1, a few faults nucleate randomly, presumably at flaws that concentrate stress. The larger faults perturb the stress field, causing new faults in their vicinity to have the same dip direction (panel 2). These faults continue to nucleate, grow, and link together until the tips of the faults from adjacent fault domains begin to overlap (panel 3). Because faults dipping in the opposite direction interfere with one another, such faults

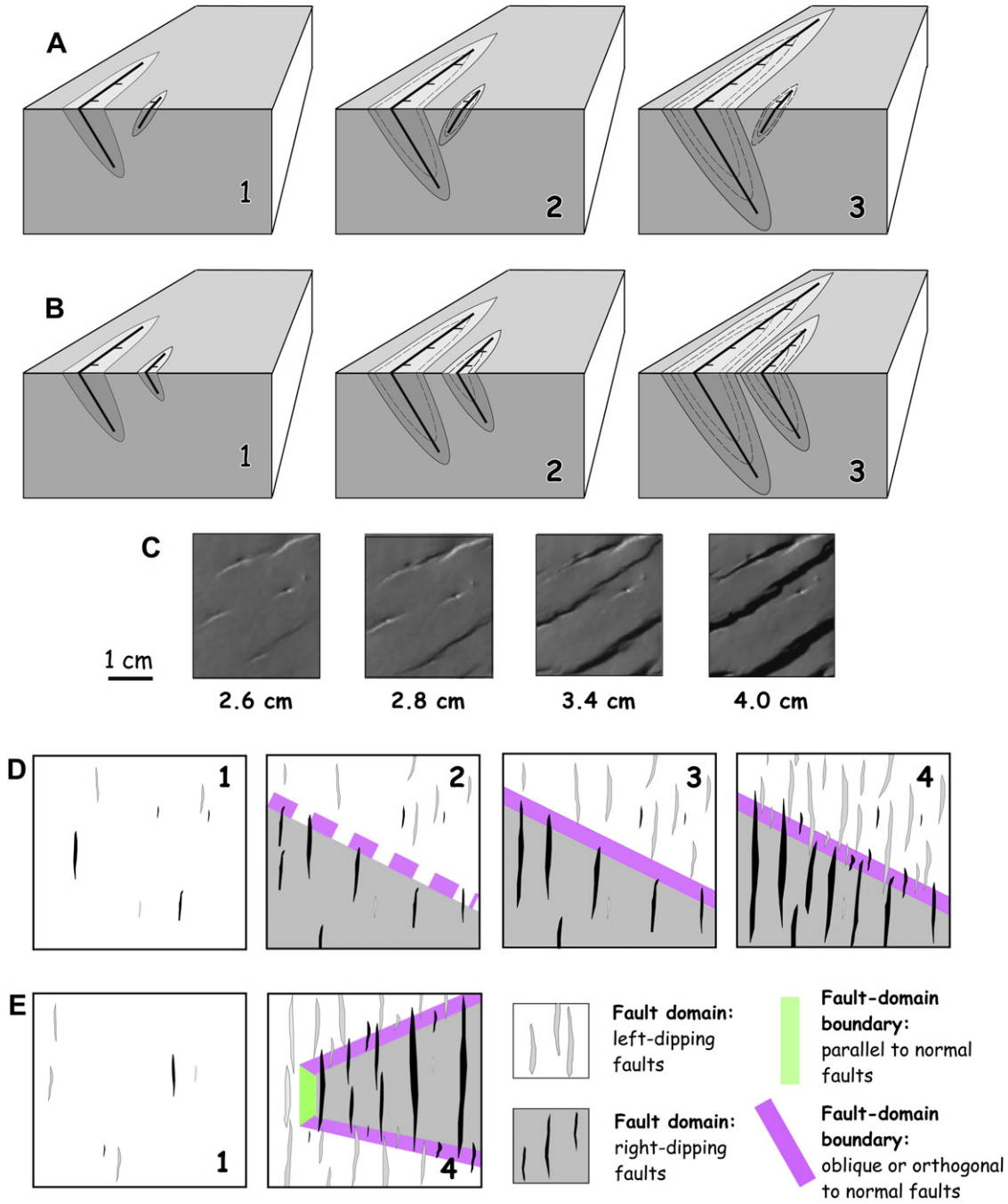

Fig. 13. Origin of fault domains and fault-domain boundaries. (A and B) Influence of stress-reduction zone on fault-domain evolution. In (A), faults have opposing dips. The smaller, left-dipping fault becomes inactive as it passes into the stress-reduction zone of the larger, right-dipping fault. In (B), both faults have same dip direction. Both faults remain active and grow because the stress-reduction zones do not overlap. (C) Example from clay model (shown in Fig. 9B) in which small, bright faults become inactive as dark faults propagate along strike and upward, become larger, and dominate the domain. (D) Scenario for the evolution (four stages) of fault domains and domain boundaries. New faults nucleate, and some become larger than others. Small faults with the opposite dip direction become inactive, and new faults have the same dip direction as the larger faults. Fault-domain boundaries develop where adjacent fault domains meet one another. (E) Alternative scenario for evolution of fault-domain boundaries. In this case, the spatial arrangement of the first-formed faults differs from that in (D), resulting in a different number of fault domains and domain boundaries. The fault-domain boundaries also have different trend from that in (D).

cannot grow appreciably in size within the fault-domain boundaries (panel 4). To accommodate additional strain, new faults develop within the fault-domain boundaries (see Figs. 5C, 8D and 9C for map-view examples and Figs. 6 and 7 for cross-section examples). These new faults may be associated with the nucleation of entirely new faults, or they may be associated with reactivation of offset fault segments, a process described by Ferrill et al. (2000). Our experimental models and many natural examples (e.g., the Pattani and Suez rift basins described above; the Timor Sea region described in Nicol et al., 1995) show that many conjugate faults result from the lateral interference of fault domains.

The number of fault domains and their domain boundaries are random, depending on the initial fault nucleation. For example, Fig. 13E shows an alternative scenario with a different spatial arrangement of the first-formed faults than that in Fig. 13D. These initial differences (panel 1) cause profound differences in the final number and arrangement of fault domains and domain

boundaries (panel 4). Furthermore, because the size and arrangement of the fault domains constrain the maximum length of faults, the size distribution of faults is likely to be different at low strains (prior to the development of fault-domain boundaries) than at higher strains. We discuss this topic in detail in a forthcoming paper.

Most fault-domain boundaries result from the juxtaposition of adjacent fault domains. Other processes, however, account for the origin of some fault-domain boundaries. Fault-domain boundaries between faulted and unfaulted regions are associated with either stress-reduction zones or differential strain. For example, the fault-domain boundaries in Fig. 1B and C are associated with stress-reduction zones near large faults. The fault-domain boundaries at the edges of the deformed zones in the models (Figs. 6–11), however, form between strained and unstrained regions. They are fault-parallel for orthogonal extension and for oblique extension when $\alpha \geq 75^\circ$ (Fig. 8A), but are fault-oblique for oblique extension when $\alpha \leq 60^\circ$ (Figs. 8B, C and 11).

5. Conclusions

1. Fault domains are a result of self-organized growth of a fault population in which the stress-reduction zones of large parallel faults are less likely to overlap and inhibit fault growth. Fault domains with their tilted fault blocks do not require special boundary conditions in experimental models. They form as a result of uniform, symmetric stretching for both orthogonal and oblique extension and in both wet clay and dry sand.
2. Most fault-domain boundaries consist of the overlapping tips of faults from adjacent fault domains, numerous fault-displacement folds, and a large number of small-scale normal faults. These boundaries are a result of the three-dimensional growth of faults and fault domains. The spatial arrangement of fault domains is governed by the spatial distribution and dip direction of the earliest formed large faults, the locations of which are, at least in part, controlled by a random distribution of flaws (nucleation points). Thus, the size and shape of fault domains and the size and orientation of fault-domain boundaries are variable.
3. The fault-domain boundaries in our models differ significantly from those in many published conceptual models of transfer/accommodation zones. In our models, fault-domain boundaries are broad zones of deformation, not discrete strike-slip or oblique-slip faults; their orientations are not systematically related to the extension direction; and they can form spontaneously without any prescribed pre-existing zones of weakness.
4. Fault-domain boundaries have two different geometries in map view: those that are parallel to the faults themselves and those that are oblique or orthogonal. The latter are associated with a large number of fault terminations. Fault-parallel and fault-oblique boundaries commonly link together and, in many cases, have a similar expression in cross-section. However, the exact cross-section geometry depends on the angle between the two linked fault-domain boundaries and the angle between the cross-section line and the fault-domain boundary (Fig. 12).
5. Natural examples of fault domains and fault-domain boundaries from the Gulf of Thailand and the Gulf of Suez closely resemble those in our experimental models.

Acknowledgments

We thank our colleagues Rolf Ackermann, Mark Baum, Roger Buck, Amy Clifton, Dan Davis, Jennifer Elder Brady, Amber Granger, Alissa Henza, and Thorsten Nagel for many valuable discussions and insights; Charlie Wall, Frank Roof, Hemal Vora, and Brian Buckman for their excellent support in the laboratory; and Nancye Dawers and David Ferrill for their constructive reviews. We also thank the Petroleum Research Fund and the National Science Foundation for their financial support of this research. Bill Chapple and Rick Groshong have had a significant influence on this research. Bill firmly believed in understanding the mechanics of geologic processes, and he passed this belief onto all of his students (including Rick and MOW). Rick valued the importance of experimental modeling, and he revived the interest of the structural-geology community (including MOW) in experimental work. We appreciate their research contributions, their leadership in the structural-geology community, and their mentorship of their students and colleagues.

References

Ackermann, R.V., Schlische, R.W., 1997. Anticlustering of small normal faults around larger faults. Geology 25, 1127–1130.
Ackermann, R.V., Schlische, R.W., Withjack, M.O., 2001. The geometric and statistical evolution of normal fault systems: an experimental study of the effects of mechanical layer thickness on scaling laws. Journal of Structural Geology 23, 1803–1819.
Angelier, J., Bergerat, F., 1983. Systemes de contrainte et extension intracontinentale. (Stress systems and continental extension). Bulletin des Centres de Recherches Exploration-Production Elf Aquitaine 7, 137–147.
Bain, G.W., Beebe, J.H., 1954. Scale model reproduction of tension faults. American Journal of Science 252, 745–754.
Bally, A.W., 1982. Musings over sedimentary basin evolution. Philosophical Transactions of the Royal Society of London A 305, 325–338.
Bellahsen, N., Daniel, J.-M., Bollinger, L., Burov, E., 2003. Influence of viscous layers on the growth of normal faults: insights from experimental and numerical models. Journal of Structural Geology 25, 1471–1485.
Brace, W.F., Kohlstedt, D.L., 1980. Limits on lithospheric stress imposed by laboratory experiments. Journal of Geophysical Research 85, 6248–6252.
Brun, J.-P., Sokoutis, D., Van Den Driessche, J., 1994. Analogue modeling of detachment fault systems and core complexes. Geology 22, 319–322.
Byerlee, J., 1978. Friction of rocks. Pure and Applied Geophysics 116, 615–626.
Carbotte, S.M., Macdonald, K.C., 1990. Causes of variation in fault-facing direction on the ocean floor. Geology 18, 749–752.
Clifton, A.E., Schlische, R.W., 2001. Nucleation, growth and linkage of faults in oblique rift zones: results from experimental clay models. Geology 29, 455–458.
Clifton, A.E., Schlische, R.W., Withjack, M.O., Ackermann, R.V., 2000. Influence of rift obliquity on fault-population systematics: results of clay modeling experiments. Journal of Structural Geology 22, 1491–1509.
Cloos, H., 1929. Experimente zur inneren tektonik. Centralblatt für Mineralogie B, 609–621.
Cloos, H., 1930. Künstliche Gebirge. Natur und Museum 59, 225–243.
Colletta, B., Le Quellec, P., Letouzy, J., Moretti, I., 1988. Longitudinal evolution of the Suez rift structure (Egypt). Tectonophysics 153, 221–233.
Cowie, P.A., Vanneste, C., Sornette, D., 1993. Statistical physics model for the spatiotemporal evolution of faults. Journal of Geophysical Research 98, 21809–21821.
Cowie, P.A., Sornette, D., Vanneste, C., 1995. Multifractal scaling properties of a growing fault population. Geophysical Journal International 122, 457–469.
Ebinger, C.J., 1989. Geometric and kinematic development of border faults and accommodation zones, Kivu-Rusizi rift, Africa. Tectonics 8, 117–133.
Eisenstadt, G., Sims, D., 2005. Evaluating sand and clay models: do rheological differences matter? Journal of Structural Geology 27, 1399–1412.
Emmons, W.H., Garrey, G.H., 1910. General geology. In: Ransome, F.L. (Ed.), Geology and Ore Deposits of the Bullfrog District. U.S. Geological Survey Bulletin, vol. 407, pp. 19–89.
Faulds, J.E., Varga, R.J., 1998. The role of accommodation zones and transfer zones in the regional segmentation of extended terranes. In: Faulds, J.E., Stewart, J.H. (Eds.), Accommodation Zones and Transfer Zones: the Regional Segmentation of the Basin and Range Province. Geological Society of America Special Paper, vol. 323, pp. 1–45.
Ferrill, D.A., Morris, A.P., Stamatakos, J.A., Sims, D., 2000. Crossing conjugate normal faults. American Association of Petroleum Geologists Bulletin 84, 1543–1559.
Gibbs, A.D., 1984. Structural evolution of extensional basin margins. Journal of the Geological Society (London) 141, 609–620.
Gupta, A., Scholz, C.H., 2000. A model of normal fault interaction based on observations and theory. Journal of Structural Geology 22, 865–879.
Handin, J., 1966. Strength and ductility. In: Clark Jr., S.P. (Ed.), Handbook of Physical Constants. Geological Society of America Memoir, vol. 97, pp. 223–289.
Higgs, W.G., McClay, K.R., 1993. Analogue sandbox modelling of Miocene extensional faulting in the outer Moray Firth. In: Williams, G.D., Dobb, A. (Eds.), Tectonics and Seismic Sequence Stratigraphy. Geological Society, Special Publication, vol. 71, pp. 141–162.

Hodgkinson, K.M., Stein, R.S., King, G.C.P., 1996. The 1954 rainbow Mountain-Fairview Peak-Dixie Valley earthquakes: a triggered normal faulting sequence. Journal of Geophysical Research 101 (B11), 25459–25472.
Hubbert, M.K., 1937. Theory of scale models as applied to the study of geologic structures. Geological Society of America Bulletin 48, 1459–1519.
Ishikawa, M., Otsuki, K., 1995. Effects of strain gradients on asymmetry of experimental normal fault systems. Journal of Structural Geology 17, 1047–1053.
Kautz, S.A., Sclater, J.G., 1988. Internal deformation in clay models of extension by block faulting. Tectonics 7, 823–832.
Kornsawan, A., Morley, C.K., 2002. The origin and evolution of complex transfer zones (graben shifts) in conjugate fault systems around the Funan Field, Pattani basin, Gulf of Thailand. Journal of Structural Geology 24, 435–449.
Lister, G.S., Etheridge, M.A., Symonds, P.A., 1986. Detachment faulting and the evolution of passive continental margins. Geology 14, 246–250.
Maltman, A., 1987. Shear zones in argillaceous sediments: an experimental study. In: Jones, M.E., Preston, R.M.F. (Eds.), Deformation of Sediments and Sedimentary Rocks. Geological Society, London, Special Publication, vol. 28, pp. 109–125.
Mandl, G., 1987. Tectonic deformation by rotating parallel faults: the "bookshelf" mechanism. Tectonophysics 141, 277–316.
McClay, K.R., 1989. Physical models of structural styles during extension. In: Tankard, A.J., Balkwill, H.R. (Eds.), Extensional Tectonics and Stratigraphy of the North Atlantic Margins. AAPG Memoir, vol. 46, pp. 95–110.
McClay, K.R., Ellis, P.G., 1987. Geometries of extensional fault systems developed in model experiments. Geology 15, 341–344.
McClay, K.R., White, M.J., 1995. Analogue modelling of orthogonal and oblique rifting. Marine and Petroleum Geology 12, 137–151.
McClay, K.R., Dooley, T., Whitehouse, P., Mills, M., 2002. 4-D evolution of rift systems: insights from scaled physical models. AAPG Bulletin 86, 935–959.
Morley, C.K., Nelson, R.A., Patton, T.L., Munn, S.G., 1990. Transfer zones in the East African rift system and their relevance to hydrocarbon exploration in rifts. AAPG Bulletin 74, 1234–1253.
Morton, W.H., Black, R., 1975. Crustal attenuation in Afar. In: Pilger, A., Rosier, A. (Eds.), Afar Depression of Ethiopia. Inter-Union Commission on Geodynamics Science Report 14. Schweizerbartische Verlagsbuchhandlung, Stuttgart, pp. 55–65.
Moustafa, A.M., 1976. Block faulting in the Gulf of Suez. In: Proceedings of the 5th Exploration Seminar. Egyptian General Petroleum Organization, Cairo.
Moustafa, A.R., 2002. Controls on the geometry of transfer zones in the Suez rift and northwest Red Sea: implications for the structural geometry of rift systems. AAPG Bulletin 86, 979–1002.
Naylor, M.A., Laroque, J.M., Gauthier, B.D.M., 1994. Understanding extensional tectonics: insights from sandbox models. In: Roure, F., Ellouz, N., Shein, V.S., Skvortsov, I. (Eds.), Geodynamic Evolution of Sedimentary Basins. International Symposium, Moscow, pp. 69–83.
Nicol, A., Walsh, J.J., Watterson, J., Bretan, P.G., 1995. Three-dimensional geometry and growth of conjugate normal faults. Journal of Structural Geology 17, 847–862.
Patton, T.L., Moustafa, A.R., Nelson, R.A., Abdine, A.S., 1994. Tectonic evolution and structural setting of the Gulf of Suez rift. In: Landon, S.M. (Ed.), Interior Rift Basins. AAPG Memoir, vol. 59, pp. 9–55.
Peacock, D.C.P., Knipe, R.J., Sanderson, D.J., 2000. Glossary of normal faults. Journal of Structural Geology 22, 291–306.
Price, N.J., Cosgrove, J.W., 1990. Analysis of Geological Structures. Cambridge University Press, New York.
Proffett Jr., J.M., 1977. Cenozoic geology of the Yerington district, Nevada, and implications for the nature and origin of Basin and Range faulting. Geological Society of America Bulletin 88, 247–266.
Richard, P., Krantz, R.W., 1991. Experiments on fault reactivation in strike-slip mode. Tectonophysics 188, 117–131.
Rutter, E.H., 1986. On the nomenclature of mode of failure transition in rocks. Tectonophysics 122, 381–387.
Schreurs, G., Buiter, S.J.H., Boutelier, D., Corti, G., Costa, E., Cruden, A.R., Daniel, J.-M., Hoth, S., Koyi, H., Kukowski, N., Lohrmann, J., Ravaglia, A., Schlische, R.W., Withjack, M.O., Yamada, Y., Cavozzi, C., DelVentisetti, C., Elder Brady, J.A., Hoffmann-Rothe, A., Mengus, J.-M., Montanari, D., Nilfouroshan, F., 2006. Analogue benchmarking: results of shortening and extension experiments. In: Geological Society, London, Special Publication, vol. 253, pp. 1–27.
Stewart, J.H., 1980. Regional tilt patterns of late Cenozoic basin-range fault blocks, western United States. Geological Society of America Bulletin 91, 460–464.
Stewart, S.A., Argent, J.D., 2000. Relationship between polarity of extensional fault arrays and presence of detachments. Journal of Structural Geology 22, 693–712.
Tron, V., Brun, J.-P., 1991. Experiments on oblique rifting in brittle-ductile systems. Tectonophysics 188, 71–84.
van der Pluijm, B.A., Marshak, S., 2004. Earth Structure, second ed. W.W. Norton, New York.
Vendeville, B., Cobbold, P.R., Davy, P., Brun, J.P., Choukroune, P., 1987. Physical models of extensional tectonics at various scales. In: Coward, M.P., Dewey, J.F., Hancock, P.L. (Eds.), Continental Extensional Tectonics. Geological Society, London, Special Publication, vol. 28, pp. 95–107.
Vendeville, B., Withjack, M., Eisenstadt, G., 1995. Introduction to Experimental Modeling of Tectonic Processes. Short Course Notes, 1995 National Meeting. Geological Society of America.
Versfelt, J., Rosendahl, B.R., 1989. Relationships between pre-rift structure and rift architecture in lakes Tanganyika and Malawi, east Africa. Nature 337, 354–356.
Weijermars, R., Jackson, M.P.A., Vendeville, B.C., 1993. Rheological and tectonic modeling of salt provinces. Tectonophysics 217, 143–174.
Wernicke, B., Burchfiel, B.C., 1982. Modes of extensional tectonics. Journal of Structural Geology 4, 105–115.
Withjack, M.O., Jamison, W.R., 1986. Deformation produced by oblique rifting. Tectonophysics 126, 99–124.
Withjack, M.O., Callaway, J.S., 2000. Active normal faulting beneath a salt layer: an experimental study of deformation in the cover sequence. AAPG Bulletin 84, 627–652.
Withjack, M.O., Schlische, R.W., 2006. Geometric and experimental models of extensional fault-bend folds. In: Geological Society, London, Special Publication, vol. 253, pp. 285–305.
Withjack, M.O., Schlische, R.W., Henza, A.A., 2007. Scaled experimental models of extension: dry sand vs. wet clay. Houston Geological Survey Bulletin 49 (8), 31–49.
Younes, A.I., McClay, K., 2002. Development of accommodation zones in the Gulf of Suez–Red Sea rift, Egypt. AAPG Bulletin 86, 1003–1026.